Separation of telomere protection from length regulation by two different point mutations at amino acid 492 of RTEL1

Riham Smoom[1], Catherine Lee May[2], Emmanuel Skordalakes[3], Klaus H. Kaestner[2] and Yehuda Tzfati[1]

[1]Department of Genetics, The Silberman Institute of Life Sciences, Safra Campus, The Hebrew University of Jerusalem, Jerusalem, 91904, Israel

[2]Department of Genetics and Institute for Diabetes, Obesity and Metabolism, Perelman School of Medicine, University of Pennsylvania, Philadelphia, PA 19104, USA

[3]Department of Pharmacology and Toxicology, Massey Cancer Center, Virginia Commonwealth University, 401 College St, Richmond, VA 23298, USA

[*]Correspondence: tzfati@mail.huji.ac.il (Y.T.) and kaestner@pennmedicine.upenn.edu (K.H.K.)

ABSTRACT

RTEL1 is an essential DNA helicase that plays multiple roles in genome stability and telomere length regulation. A variant of RTEL1 with a lysine at position 492 is associated with short telomeres in *Mus spretus*, while a conserved methionine at this position is found in *M. musculus,* which has ultra-long telomeres. In humans, a missense mutation at this position (*RTEL1*^{M492I}) causes a fatal telomere biology disease termed Hoyeraal-Hreidarsson syndrome (HHS). We previously described a *M. musculus* mouse model termed 'Telomouse', in which changing methionine 492 to a lysine (M492K) shortened the telomeres to their length in humans. Here, we report on the derivation of a mouse strain carrying the M492I mutation, termed 'HHS mouse'. The HHS mouse telomeres are not as short as those of Telomice but nevertheless they display higher levels of telomeric DNA damage, fragility and recombination, associated with anaphase bridges and micronuclei. These observations indicate that the two mutations separate critical functions of RTEL1: M492K mainly reduces the telomere length setpoint, while M492I predominantly disrupts telomere protection. The two mouse models enable dissecting the mechanistic roles of RTEL1 and the different contributions of short telomeres and DNA damage to telomere biology diseases, genomic instability, cancer, and aging.

INTRODUCTION

Telomeres are repetitive sequences bound by specialized proteins that protect chromosome ends from deleterious activation of the canonical DNA damage response (DDR) (reviewed in[1]). In all vertebrates, telomeres consist of 5'-TTAGGG-3' DNA repeats, and end with an essential single-stranded 3'-overhang. This overhang can be elongated by the enzyme telomerase to compensate for sequence loss due to the end replication problem and end-processing events. Telomerase synthesizes *de novo* telomeric repeats (TTAGGG) at chromosome ends using an integral RNA (termed TER or TR) and a telomerase reverse transcriptase (TERT) subunit that copies a short template sequence from the RNA component onto the telomere 3'end[2]. Human TERT (hTERT) expression is suppressed in most human somatic tissues; consequently, telomeres gradually shorten with each cell division. When even a few telomeres in a given cell become critically short, they trigger a DNA damage signal and cellular senescence. Very short or otherwise unprotected telomeres can induce genomic instability, accumulation of mutations and a stress response, which are drivers of cancer and age-related diseases[3-5].

The large difference in telomere length between two closely related and inter-breedable species of mice, *M. musculus* and *M. spretus,* was shown to be associated with a single locus encoding a DNA helicase, which was consequently termed 'regulator of telomere elongation 1' (RTEL1)[6]. Indeed, RTEL1 was found as a dominant factor regulating telomere length and was suggested to facilitate telomere extension by telomerase in a yet unknown mechanism[6-9].

RTEL1 is an essential DNA helicase from the XPD family helicases, which contain a conserved iron-sulfur cluster domain, translocate on ssDNA in a 5'-3' direction, and play important roles in genome stability[10-12]. Also RTEL1, in addition to its role in telomere length regulation, was suggested to play multiple roles in telomeric, as well as non-telomeric, genome stability: It associates with the replisome through binding to proliferating cell nuclear antigen (PCNA) to facilitate both genome-wide and telomeric replication[13]; it is recruited to the telomeres by TRF1 to resolve G4 quadruplexes and prevent telomere fragility[14]; it is recruited to telomeres by TRF2 in S phase to promote t-loop unwinding and prevent stabilization of reversed replication forks by telomerase[15-17]; and it stabilizes long G-overhangs in cells overexpressing telomerase[18]. In addition, it is involved in non-coding RNA metabolism: it facilitates pre-U2 snRNA trafficking between the nucleus and cytoplasm[19] and the abundance and localization of the telomeric long non-coding RNA TERRA[20].

heterozygous carriers of *RTEL1* mutations display increased genomic instability and an elevated risk for cancer and pulmonary fibrosis[21-23]. Biallelic *RTEL1* germline mutations cause a severe telomere biology disease (TBD) named Hoyeraal-Hreidarsson syndrome (HHS)[24-28]. HHS is a severe form of dyskeratosis congenita, characterized by accelerated telomere shortening and diverse clinical symptoms including immunodeficiency, neurodevelopmental defects, and bone marrow failure[29]. While accelerated telomere shortening is thought to be the main cause for the disease, the contribution of other manifestations of RTEL1 dysfunction to the diverse clinical symptoms remains to be explored.

We have previously found an HHS-causing mutation in a conserved methionine at position 492 of *RTEL1* (M492I)[26]. The HHS patients were compound heterozygous for this mutation, *RTEL1*^{M492I}, in combination with a nonsense mutation, *RTEL1*^{R972X}, that leads to mRNA degradation by the nonsense-mediated decay pathway[26]. Telomeres were severely short in leukocytes of the patients, but not in primary fibroblasts[30]. Yet, primary patient fibroblasts displayed diminished telomeric overhangs and increased DNA damage foci colocalizing with telomeres, pointing to a defect in telomere structure that compromised telomere protection rather than length[30]. The ectopic expression of a 544 amino-acid long variant of TPP1 (TPP1-L), which does not facilitate telomere elongation, rescued the viability of patient fibroblasts expressing ectopic hTERT while their telomeres continued to shorten. Altogether, these observations suggested a defect in telomere structure, in addition to excessive telomere shortening in the blood, in these HHS patients[8,30].

A natural variation at the same position of RTEL1 in *M. spretus* (M492K) shortened the telomere length setpoint when introduced into *M. musculus,* generating a mouse strain with human-length telomeres termed 'Telomouse'[9]. The structure and function of the Telomouse telomeres appear normal, consistent with the natural presence of the K492 variation in *M. spretus*[9]. Here, we derived an additional *Rtel1* mutant mouse strain, which is homozygous for the HHS-causing mutation (M492I), and termed it 'HHS mouse'. We hypothesized that a mouse carrying the HHS-causing mutation in *Rtel1* would model the consequences of telomere dysfunction and genomic instability found in HHS patients, including telomere length-independent DNA damage. We find that the HHS mouse exhibits only moderate shortening of telomere repeats but instead shows impaired telomere protection, indicating that the two *Rtel1* mutations affect different functions of RTEL1 in telomere length regulation and telomere structure.

RESULTS

Derivation of the HHS mouse model

The sequence of the RTEL1 helicase domains 1 and 2 (HD1 and HD2), and the iron-sulfur (FeS) and ARCH domains, is highly conserved between human and mouse (Figures 1a, b and S1). Specifically, methionine 492 is conserved in vertebrates with only a few naturally occurring exceptions: a leucine found in this position in several cat species, and a lysine in *M. spretus*[9,26]. To test the effect of the M492I HHS-causing mutation in the mouse, we derived a *M. musculus* strain with this mutation using CRISPR-Cas9 assisted genome editing in zygotes (Figure 1c). We employed the Cas9 nickase (D10A Cas9 mutant) enzyme and two guide RNAs to generate nicks on both strands of the *Rtel1* gene to facilitate gene conversion using a repair template (Figure 1c). Successful gene targeting in the resulting offspring was confirmed by DNA sequencing (Figure 1d). This founder mouse was backcrossed to the isogenic parental wild-type (WT) C57BL/6 mice to generate F0 mice heterozygous for the *Rtel1*^{M492I} allele, termed *Rtel1*$^{M/I}$. F0 *Rtel1*$^{M/I}$ mice were crossed to C57BL/6 mice two additional times to generate F1 and F2 *Rtel1*$^{M/I}$ mice. Homozygosity for the *Rtel1* mutation (*Rtel1*$^{I/I}$) was established in the third generation (F3). The homozygous *Rtel1*$^{I/I}$ mice were then bred *inter se* for eleven additional generations up to F14 to date, and were analyzed for telomere length and function. We termed the *Rtel1*$^{I/I}$ mouse model 'HHS mouse'.

The HHS mutation causes telomere shortening in human and mouse fibroblasts

Telomerase positive HHS patient cells such as EBV transformed lymphoblastoid cell lines (LCLs) and primary fibroblasts expressing ectopic hTERT display progressive telomere shortening despite the presence of catalytically-active telomerase[8,26,30]. This telomere shortening was suppressed by ectopic expression of WT RTEL1[8,26]. To examine the rate of telomere shortening caused by RTEL1-deficiency in human cells, we used telomerase-positive patient fibroblasts harboring the *RTEL1*^{M492I} mutation and an inducible ectopic copy of the WT 1,300 amino-acid variant of human RTEL1 (RTEL1v2). The induced expression of RTEL1v2 by adding doxycycline to the medium elongated their telomeres[8]. Omitting doxycycline from the medium silenced the ectopic RTEL1v2 and resulted in gradual telomere shortening over 100 population doublings (PD) (Figure S2b). Silencing RTEL1v2 slowed down cell growth after 60 PD without doxycycline and changed cell morphology, as compared to the RTEL1v2-expressing cells, (Figure S2a, c). We determined the mean telomeric restriction fragments (TRF) length (MTL) every 10

PD by the in-gel hybridization method[8,9]. While the MTL was stable in the cells expressing RTEL1v2 (DOX+), it shortened gradually upon silencing RTEL1v2 from 12.3 kb at PD 10 to 6.4 kb at PD100, indicating an average telomere shortening of 65 nt per PD (Figure S2b).

To examine if the *Rtel1*^{M492I} mutation has a similar effect on telomere length in the mouse, we established mouse embryonic fibroblasts (MEFs) from heterozygous (M/I), homozygous (I/I) and control (M/M*) F3 littermate embryos generated by intercrossing F2 *Rtel1*$^{M/I}$ mice. As another control, we used WT (M/M) MEFs generated by breeding WT mice that did not harbor the *Rtel1*^{M492I} mutation in their pedigree ancestors, avoiding trans-generational inheritance of short telomeres from the heterozygous mice to the WT offspring. MEF cultures were established by serial passaging and selection for spontaneous immortalization, and followed in culture over 250 PD. The genotypes of the MEFs were reconfirmed at PD 250 by PCR and differential digestion of the *Rtel1*^{M492I} allele by *HinfI* (Figure S3). During growth, the cultures passed several crisis periods and one to three transition points in which the MEFs increased their growth rates and changed their cellular morphology (Figures S4). All MEF lines were immortalized by PD 70 and their shapes became rounder. During the final growth phase, the M/I, I/I, M/M* and M/M MEF cultures grew at the same average rate, about one PD/day (Figure S4).

We examined the TRF length for these four cultures at multiple PD levels by in-gel hybridization (Figure 2a). Each sample was assayed several times in independent gels (Figure 2b and Extended Data Table 1). The average MTL of all MEFs cultures shortened during the initial growth phase until immortalization occurred at about PD 70 (arrows in Figure 2), presumably due to the lower telomerase activity present in MEFs prior to immortalization[9,31]. After immortalization, MTL of the WT and M/I cultures stabilized, while the I/I MTL continued to shorten at an average rate of ~35 bp per PD to 23.7 kb at PD 250, as compared with the WT (M/M) MTL of 37.8 kb (Figure 2). The M/M* MEFs had shorter MEFs MTL of 29.7 kb at PD 10, presumably due to the inheritance of short telomeres from the heterozygous parents, which shortened to 26.6 kb at PD 250. Altogether, the *mRtel1*^{M492I} mutation caused gradual telomere shortening in mouse fibroblasts, phenocopying the telomere shortening observed in human HHS patients carrying the same mutation. The telomere shortening was significantly milder in the I/I MEFs than in the K/K MEFs, reaching a MTL of 23.7 kb at PD 250, as compared to 14.7, respectively[9]. Also, the telomere shortening of the heterozygous M/I MEFs was significantly milder than that of the M/K MEFs. Altogether, these results suggest that the effect of the M492I on telomere length regulation function of RTEL1 is less severe than the effect of the M492K mutation, consistent with the

more conservative nature of the substitution of methionine to isoleucine, both comprised of a hydrophobic side chain, than to the positively charged lysine.

The HHS mutation impairs telomere protection and genome stability

One central role of telomeres is to suppress the DNA damage response (DDR) at chromosome ends and prevent the consequent cell cycle arrest and deleterious fusions of chromosomes[1]. Telomere dysfunction can occur either as a result of telomere shortening beyond a critical length or via damage to the telomere structure. The HHS mutation *Rtel1*^{M492I} results in milder telomere shortening than the more radical *Rtel1*^{M492K} mutation, raising the question whether the *Rtel1*^{M492I} mutation causes defects other than telomere shortening that contribute to HHS etiology. In fibroblasts derived from HHS patients, the *Rtel1*^{M492I} mutation was associated with activation of DDR at telomeres even without telomere shortening, suggesting the presence of a length-independent defect in telomere structure and function[30].

DNA damage response foci that colocalize with telomeres are termed telomere dysfunction-induced foci (TIF) and are considered a hallmark of telomere failure. We studied the presence of telomeric and genome-wide DDR foci in the I/I MEFs using antibodies against the DDR marker γH2AX and the telomere protein TRF2, and compared them to K/K and M/M (WT) MEFs (Figure 3). The overall (genome-wide) levels of DDR were high in all MEF cultures regardless of genotype (Figure 3a, b), as shown previously for MEFs growing under atmospheric oxygen levels[9,32]. There was no significant difference in the abundance of DDR foci between the I/I MEFs and the K/K or M/M MEFs (Figure 3b). Some of the cells displayed overt damage throughout the nucleus without visible distinct foci, and the frequency of these cells was somewhat higher in the I/I MEFs (7%) than the K/K (5%) or the WT (4%) MEFs (Figure 3d, e). DNA damage at telomeres, however, was specifically elevated in I/I but not K/K MEFs, as revealed by the significant increase in the number of TIF foci (Figure 3c). Also elevated were micronuclei and anaphase bridges, which are known to associate with telomere dysfunction and genome instability (Figure 3d, e)[4]. Altogether, these results suggest that the I/I MEFs telomeres, although longer than those of K/K MEFs, are nevertheless deprotected and compromised in their ability to suppress the DDR and prevent genomic instability. Since in interphase cells we can only observe telomeres with sufficient length and detectable telomeric signal, we studied TIF formation also in metaphase-arrested cells where individual chromosomes and their ends can be visualized by DAPI

staining, telomeric repeats by FISH with a telomeric PNA probe, and DDR foci by immunofluorescence for γH2AX (Figure 4). Analyzing TIF in metaphase chromosomes of the I/I MEFs revealed that most of them were found in chromosome ends with detectable FISH signal and not at signal-free chromosome ends (Figure 4a), suggesting that the *Rtel1*^{M492I} mutation caused a defect in telomere structure or composition that resulted in the activation of DDR at telomeres with sufficient length to be detected by FISH. In addition, we observed among the I/I MEFs an increased level of anaphase bridges, in which at least one of the two bridged nuclei displayed overt DDR (Figure 4b).

RTEL1 dysfunction in patient cells and mouse *Rtel1* null cells was reported to induce telomere aberrations, such as telomere loss, telomere fragility, interstitial telomere insertion (ITS) and telomere fusion (reviewed in[12]). To examine the frequency of telomere aberrations caused by the HHS *Rtel1*^{M492I} mutation, we performed metaphase FISH on MEFs cultures PD 250 (Figure 5). The most significant phenotype was an increase in telomere fragility in the I/I MEFs as compared to the M/M control (Figure5b, c), consistent with the increased frequency of TIF in these MEFs (Figure 4) and pointing to increased telomeric replication stress. The I/I MEFs displayed additional phenotypes associated with genomic instability, which could result from telomeric DNA damage, such as anaphase bridges, connected nuclei, micronuclei, chromosome fragments, and mitotic catastrophe (Figures 3d, e and 5d-f).

Telomere sister chromatid exchange (T-SCE), indicating elevated homologous recombination events between sister telomeres, was reported in RTEL1-deficient HHS patient cells[27]. We examined the frequency of T-SCE events in the I/I MEFs by chromatid-orientation FISH (CO-FISH), differentiating between the leading and lagging telomeres by labeling them with green and red strand-specific PNA probes. T-SCE appears as colocalization of the two probes at the same telomere end (Figure 6). We observed a significant increase in T-SCE events in the I/I MEFs compared to control M/M MEFs (Figure 6c), indicating increased homologous recombination at the telomeres of the I/I MEFs, which was not detected in the K/K MEFs of the same PDs[9]. Altogether, these results suggest that the defects caused by the two mutations are different; while the *Rtel1*^{M492K} mutation dramatically reduces the telomere length setpoint but maintains functional protected telomeres, the *Rtel1*^{M492I} mutation shortens telomeres to a lesser extent but impairs telomere protection and genome stability.

Short telomeres in the HHS mouse

To examine the effect of the *Rtel1*^{M492I} mutation on somatic tissues of HHS mice, we measured the telomere length in blood and tail DNA samples over several generations (F3 to F10 in blood and F3 to F11 in tail) and compared the results to Telomice (K/K) and WT (M/M) control mice (Figure 7). In blood, the MTL shortened to an average length of 27.9 kb in F8 HHS mice and no significant further shortening was observed through F10, as compared to 40.1 kb in WT samples (Extended Data Table 2 and Figures 7a, c, and S5). In tail samples, MTL shortened to an average of 29.0 kb in F6 HHS mice and no further shortening was observed through F11, as compared to 42.3 kb in the WT samples (Extended Data Table 2 and Figures 7b, d, and S5). These results indicate that the telomeres in the HHS mouse germline had stabilized on a new telomere length set point that is significantly longer than the new setpoint reached in Telomice F16 (16.7 kb and 19.2 kb in blood and tail, respectively; Figure 7c, d)[9].

T-circles excision is not the major cause for the HHS mouse telomeric phenotypes

The excision of telomere (t)-loops in the form of telomeric (t)-circles has been suggested to cause telomere loss in RTEL1-deficient mouse cells[15,16,33]. Such a process could result not only in telomere shortening but also in the induction of DDR due to broken telomere ends. To determine whether increased t-loop excision contributed to telomere shortening and aberrations in HHS mice, we examined the abundance of t-circle in tail samples by two-dimensional (2D) PFGE (Figure S6) but found no significant increase in t-circle formation in the HHS mouse, as compared to Telomice at the same generation (F5) and to WT control mice. These results were consistent with the results obtained in the patient cells[26], excluding t-loop excision as a major cause for telomere shortening, DNA damage response activation and telomere aberrations observed in HHS mouse and patient cells.

DISCUSSION

RTEL1 has been implicated in diverse pathways essential for genome maintenance and stability, particularly in telomere maintenance and length regulation (reviewed in[12]). Mutations in *RTEL1* cause diverse symptoms in telomere biology diseases (TBDs) such as HHS and pulmonary fibrosis, and in cancer predisposition[12]. RTEL1-dysfunction in patient cells was associated with severe telomere shortening but also with increased telomeric damage, telomere aberrations and genomic instability, even in cells with normal telomere length[8,22,30]. These diverse symptoms and molecular phenotypes

raise the question whether defects other than telomere shortening also contribute to disease etiology[12]. We have shown previously that changing methionine 492 of *Rtel1* to a lysine in a *M. musculus* mouse model termed 'Telomouse' shortened its telomeres to the length of human telomeres[9]. The Telomouse telomeres do not display elevated DDR, fragility or other telomere aberrations, except for telomere loss and Robertsonian fusions[9]. These observations suggest that these telomeres are largely protected unless becoming critically short and induce fusions between the two short (p) arms of the acrocentric mouse chromosomes (Robertsonian fusions), which are tolerated because of the proximity of the two centromeres in the fused dicentric chromosome[34]. Thus, the *Rtel1*^{M492K} mutation mostly affected the telomere length regulation function of RTEL1. Here we report on another mouse model, carrying the HHS causing mutation *Rtel1*^{M492I}, termed HHS mouse, which exhibits a distinct phenotype.

Using the structure prediction model *Alphafold*[35], we find that the helicase domains of human and mouse RTEL1 are almost identical (Figure 8). The substitution of a methionine by an isoleucine is the most conservative substitution of a protein residue. However, there is a distinct difference between an isoleucine and methionine and that is the methionine sulfur atom. It has been shown that the sulfur atom of methionine allows for hydrophobic contacts over a longer distance than a carbon atom (5.5Å *versus* 4.5Å)[36]. As a result, the methionine interactions with the surrounding residues provide an additional 1-1.5Kcal/mol stabilization to the protein[36]. Methionine 492 is buried at the center of the RTEL1 helicase domain and it is important for its proper folding (Figure 8a). The structure model of the complex of the single-stranded DNA bound to the helicase domain shows two hydrogen bonds between each of the residues K257 and E261 and the DNA substrate (Figure 8 b, c, d). The helix formed by these residues is adjacent to the helix of M492 and makes direct hydrophobic contact with it via V255 and the aliphatic portion of the sidechain of E256 (Figure 8c, d). The introduction of an isoleucine in position of M492 is predicted to destabilize this region, affecting DNA binding and processing, and leading a to partially defective RTEL1 helicase core. In addition, the M492I mutation was reported to compromise the interaction of RTEL1 with DNA Polymerase Delta Interacting Protein 3 (PolDIP3)[37]. The RTEL1 structure model shows that the edge of the helix that includes M492 but on the opposite side of it, is solvent exposed and therefore available for interactions (Figure 8e, f). The M492I mutation destabilizes this region, which in turn may subtly affect POLDIP3 binding. This is further supported by our model which places all three residues reported as important for the RTEL1-POLDIP3 interaction (M492, L710 and G739) on the same surface of the RTEL1 protein[37] (Figure 8e, f). A striking difference between the

human and mouse RTEL1 involving the helix formed by M492 is the residue at position 485. In the case of human RTEL1 it is a valine while in the case of mouse it is a leucine, which has a longer side chain. An overlay of the human and mouse RTEL1 helicase domains (Figure 8b) shows that the longer leucine 485 sidechain of the mouse RTEL1 places the M492 helix further away from the helix containing the DNA interacting residues K257 and E261. This helix position places the mouse M492 approximately 1.0Å further away from the interacting residues V255 and E256. We hypothesize that due to this increased distance, the introduction of M492I may be more destabilizing to the mouse RTEL1 than to the human protein.

The telomeres of HHS mice and MEFs shortened gradually, but to a lesser extent than those of Telomouse (Figures 2, 7 and S5, and Extended Data Tables 1 and 2). Nevertheless, telomere protection in the HHS (I/I) MEFs was compromised more than in Telomouse (K/K) MEFs, as indicated by the increased levels of DDR, telomere fragility, anaphase bridges, micronuclei, and telomere sister chromatid exchange (T-SCE) (Figures 3-6). On the other hand, telomere loss and Robertsonian fusions were elevated in the Telomouse MEFs due to the more severe telomere shortening caused by the M492K mutation[9]. Telomere shortening in both Telomouse and the HHS mouse was not associated with increased formation of t-circles (Figure S6), ruling out t-loop excision as a major cause for telomere shortening and aberrations, consistently with the results obtained for HHS patient cells[8,26].

In sum, our results show that the M492I mutation causes milder telomere shortening but a more severe telomere protection defect than the M492K mutation, distinguishing two separate functions of RTEL1. We can speculate that the two substitutions have different effects on the structure of the helicase core, the single-stranded DNA binding, and protein interactions. Yet, the mechanistic details of how they affect telomere length and telomere protection differently are yet to be explored. The observations in cells of HHS patients and the HHS mouse support the notion that not only telomere shortening but also length-independent telomere dysfunction contribute to the HHS etiology. While accelerated telomere shortening may take years to reach critically short lengths and cause disease, defects in telomere structure and function may affect physiology more immediately. Therefore, such length-independent effects on telomere function can explain the more severe symptoms and earlier onset of HHS as compared with dyskeratosis congenita, which is thought to result from telomerase deficiency and telomere shortening. The HHS mouse and Telomouse will serve as invaluable models to study the mechanistic functions of RTEL1 in telomere length regulation and protection and the

consequences of the disruption of these functions on the organismal physiology in telomere biology disease, normal aging, and cancer.

Acknowledgements

This research was supported in parts by the Israel Science Foundation grants 2071/18 and 1342/23 to Y.T., the NIDDK through R37-DK053839 and R01-CA249929 to K.H.K., and by the Israel-UK-Palestine GROWTH Fellowship to R.S. We are grateful to all members of the Tzfati and Kaestner laboratories for stimulating discussions and assistance. We thank Ittai Ben-Porath and Amir Eden for the gifts of WT mice and MEFs; Mark Tigue for the maintenance of the mouse colony; Devora Olam for assistance in mouse blood collection; Adan Mhameed for assistance in quantifying FISH aberrations; Naomi Melamed-Book, Bio-Imaging Unit at The Hebrew University; Dana Avrahami-Tzfati for assistance with CRISPR editing in zygotes; and Ran Avrahami for assistance with statistical analyses.

AUTHOR CONTRIBUTIONS

Corresponding authors Y.T. (telomere biology) and K.H.K. (mouse biology): Y.T. K.H.K.: study concept and design; analysis and interpretation of data; writing and revising the manuscript. R.S.: study concept and design; Performing experiments; analysis of telomere phenotypes; interpretation of data; writing and revising the manuscript; C.L.M.: derivation of the mouse strains; E.S.: computational analysis of the mouse and human RTEL1 protein structure.

REFERENCES

1. de Lange, T. Shelterin-Mediated Telomere Protection. *Annu Rev Genet* **52**, 223-247 (2018).
2. Blackburn, E.H. & Collins, K. Telomerase: an RNP enzyme synthesizes DNA. *Cold Spring Harb Perspect Biol* **3**(2011).
3. Lansdorp, P.M. Telomeres, aging, and cancer: the big picture. *Blood* **139**, 813-821 (2022).
4. Nassour, J., Przetocka, S. & Karlseder, J. Telomeres as hotspots for innate immunity and inflammation. *DNA Repair (Amst)* **133**, 103591 (2024).
5. Nassour, J., Schmidt, T.T. & Karlseder, J. Telomeres and Cancer: Resolving the Paradox. *Annu Rev Cancer Biol* **5**, 59-77 (2021).
6. Ding, H. *et al.* Regulation of murine telomere length by Rtel: an essential gene encoding a helicase-like protein. *Cell* **117**, 873-86 (2004).

7. Uringa, E.J. *et al.* RTEL1 contributes to DNA replication and repair and telomere maintenance. *Mol Biol Cell* **23**, 2782-2792 (2012).

8. Awad, A. *et al.* Full length RTEL1 is required for the elongation of the single-stranded telomeric overhang by telomerase. *Nucleic Acids Res* **48**, 7239-7251 (2020).

9. Smoom, R. *et al.* Telomouse-a mouse model with human-length telomeres generated by a single amino acid change in RTEL1. *Nat Commun* **14**, 6708 (2023).

10. Cheng, K. & Wigley, D.B. DNA translocation mechanism of an XPD family helicase. *Elife* **7**(2018).

11. Estep, K.N. & Brosh, R.M., Jr. RecQ and Fe-S helicases have unique roles in DNA metabolism dictated by their unwinding directionality, substrate specificity, and protein interactions. *Biochem Soc Trans* **46**, 77-95 (2018).

12. Hourvitz, N., Awad, A. & Tzfati, Y. The many faces of the helicase RTEL1 at telomeres and beyond. *Trends Cell Biol* (2023).

13. Vannier, J.B. *et al.* RTEL1 is a replisome-associated helicase that promotes telomere and genome-wide replication. *Science* **342**, 239-42 (2013).

14. Sfeir, A. *et al.* Mammalian telomeres resemble fragile sites and require TRF1 for efficient replication. *Cell* **138**, 90-103 (2009).

15. Sarek, G. *et al.* CDK phosphorylation of TRF2 controls t-loop dynamics during the cell cycle. *Nature* **575**, 523-527 (2019).

16. Sarek, G., Vannier, J.B., Panier, S., Petrini, J.H. & Boulton, S.J. TRF2 recruits RTEL1 to telomeres in S phase to promote t-loop unwinding. *Mol Cell* **57**, 622-35 (2015).

17. Margalef, P. *et al.* Stabilization of Reversed Replication Forks by Telomerase Drives Telomere Catastrophe. *Cell* **172**, 439-453 e14 (2018).

18. Porreca, R.M. *et al.* Human RTEL1 stabilizes long G-overhangs allowing telomerase-dependent over-extension. *Nucleic Acids Res* **46**, 4533-4545 (2018).

19. Schertzer, M. *et al.* Human regulator of telomere elongation helicase 1 (RTEL1) is required for the nuclear and cytoplasmic trafficking of pre-U2 RNA. *Nucleic Acids Res* **43**, 1834-47 (2015).

20. Ghisays, F. *et al.* RTEL1 influences the abundance and localization of TERRA RNA. *Nat Commun* **12**, 3016 (2021).

21. Cogan, J.D. *et al.* Rare variants in RTEL1 are associated with familial interstitial pneumonia. *Am J Respir Crit Care Med* **191**, 646-55 (2015).

22. Marsh, J.C.W. *et al.* Heterozygous RTEL1 variants in bone marrow failure and myeloid neoplasms. *Blood Adv* **2**, 36-48 (2018).

23. Hassani, M.A., Murid, J. & Yan, J. Regulator of telomere elongation helicase 1 gene and its association with malignancy. *Cancer Rep (Hoboken)* **6**, e1735 (2023).

24. Ballew, B.J. *et al.* A recessive founder mutation in regulator of telomere elongation helicase 1, RTEL1, underlies severe immunodeficiency and features of Hoyeraal Hreidarsson syndrome. *PLoS Genet* **9**, e1003695 (2013).

25. Ballew, B.J. *et al.* Germline mutations of regulator of telomere elongation helicase 1, RTEL1, in Dyskeratosis congenita. *Hum Genet* **132**, 473-80 (2013).

26. Deng, Z. *et al.* Inherited mutations in the helicase RTEL1 cause telomere dysfunction and Hoyeraal-Hreidarsson syndrome. *Proc Natl Acad Sci U S A* **110**, E3408-16 (2013).

27. Le Guen, T. *et al.* Human RTEL1 deficiency causes Hoyeraal-Hreidarsson syndrome with short telomeres and genome instability. *Hum Mol Genet* **22**, 3239-49 (2013).

28. Walne, A.J., Vulliamy, T., Kirwan, M., Plagnol, V. & Dokal, I. Constitutional mutations in RTEL1 cause severe dyskeratosis congenita. *Am J Hum Genet* **92**, 448-53 (2013).

29. Glousker, G., Touzot, F., Revy, P., Tzfati, Y. & Savage, S.A. Unraveling the pathogenesis of Hoyeraal-Hreidarsson syndrome, a complex telomere biology disorder. *Br J Haematol* **170**, 457-71 (2015).

30. Lamm, N. *et al.* Diminished telomeric 3' overhangs are associated with telomere dysfunction in Hoyeraal-Hreidarsson syndrome. *PLoS One* **4**, e5666 (2009).

31. Prowse, K.R. & Greider, C.W. Developmental and tissue-specific regulation of mouse telomerase and telomere length. *Proc Natl Acad Sci U S A* **92**, 4818-22 (1995).

32. Di Micco, R. *et al.* DNA damage response activation in mouse embryonic fibroblasts undergoing replicative senescence and following spontaneous immortalization. *Cell Cycle* **7**, 3601-6 (2008).

33. Vannier, J.B., Pavicic-Kaltenbrunner, V., Petalcorin, M.I., Ding, H. & Boulton, S.J. RTEL1 Dismantles T Loops and Counteracts Telomeric G4-DNA to Maintain Telomere Integrity. *Cell* **149**, 795-806 (2012).

34. Sanchez-Guillen, R.A. *et al.* On the origin of Robertsonian fusions in nature: evidence of telomere shortening in wild house mice. *J Evol Biol* **28**, 241-9 (2015).

35. Jumper, J. *et al.* Highly accurate protein structure prediction with AlphaFold. *Nature* **596**, 583-589 (2021).

36. Valley, C.C. *et al.* The methionine-aromatic motif plays a unique role in stabilizing protein structure. *J Biol Chem* **287**, 34979-34991 (2012).

37. Bjorkman, A. *et al.* Human RTEL1 associates with Poldip3 to facilitate responses to replication stress and R-loop resolution. *Genes Dev* **34**, 1065-1074 (2020).

38. Gohring, J., Fulcher, N., Jacak, J. & Riha, K. TeloTool: a new tool for telomere length measurement from terminal restriction fragment analysis with improved probe intensity correction. *Nucleic Acids Res* **42**, e21 (2014).

39. Yang, H., Wang, H. & Jaenisch, R. Generating genetically modified mice using CRISPR/Cas-mediated genome engineering. *Nat Protoc* **9**, 1956-68 (2014).

40. Kelley, L.A., Mezulis, S., Yates, C.M., Wass, M.N. & Sternberg, M.J. The Phyre2 web portal for protein modeling, prediction and analysis. *Nat Protoc* **10**, 845-58 (2015).

FIGURE LEGENDS

Figure 1. Derivation of the Rtel1^{M492I} allele by CRISPR-Cas9 nickase editing. (a) A scheme showing the helicase domains (HD1 and HD2), the iron-sulfur cluster (FeS), the nuclear localization signal (NLS), harmonin N-like domains (HNL1 and HNL2), PCNA-interacting protein (PIP) motif, and the C4C4 ring-finger domain[12] of RTEL1. (b) RTEL1 protein and DNA sequence alignment showing codon 492 (boxed) and flanking sequences in human and mouse. Variations in mouse from the human sequence are shown in green and mutations in HHS patients and mouse models are shown in red. The mean telomeric restriction fragment (TRF) length (MTL) values measured by the in-gel hybridization method are indicated for human and mouse. (c) Illustration showing the WT allele, the two positions targeted by gRNAs (blue and red arrowheads), the ssDNA repair template with the mutation, left homology arm (blue), right homology arm (red), and the resulting targeted allele. (d) Sanger sequencing of the HHS line founder confirming the replacement of the 'G' with a 'T' in codon 492, changing the methionine to an isoleucine (underlined).

Figure 2. Telomeres of MEFs carrying the homozygous *Rtel1*^{M492I} mutation progressively shorten with cell division in culture. MEFs cultures were prepared from F3 littermate embryos, I/I, M/I and M/M*, generated by mating F2 heterozygous mice carrying the Rtel1 M492I mutation. Another control M/M MEFs culture (M/M) was generated by intercrossing WT mice which did not have any Rtel1 mutation in their pedigree, to avoid trans-generational inheritance of short telomeres from heterozygous *Rtel1* mutant mice to the WT offspring. All four cell lines were immortalized by serial passaging and grown to PD 250. (a) Genomic DNA samples extracted from the indicated MEFs cultures and PDs were digested by *HinfI* restriction endonuclease and analyzed by PFGE and in-gel hybridization with a C-rich telomeric probe. Shown is the hybridization after denaturation (see Methods). Mean TRF length (MTL) was quantified for each sample by *TeloTool*[38] and indicated below the lanes. (b) All MTL values measured in multiple gels for the same M/M, I/I, and M/I MEFs samples were plotted, in addition to K/K and M/K MEFs results from[9], for comparison.

Figure 3**. The HHS mutation impairs telomere protection and genome stability.** (a) The formation of DNA damage response foci and their localization to telomeres (defined as TIF) in interphase nuclei were

examined by immunofluorescence staining with antibodies detecting the DDR marker γH2AX (green) and the telomere protein TRF2 (red). Scatter plots show the number of DDR foci (b) and TIF (c) per nucleus. A total of 110 M/M, 110 K/K, and 153 (b) or 182 (c) of I/I nuclei were countified for MEFs PD 102. All three MEFs cultures were analyzed side by side; the results for the K/K and control (M/M) MEFs appeared in[9]. The mean values and SDs are indicated by black lines, and P values were calculated by unpaired t-test. (d) Representative images showing nuclei with overt DDR (d1,2), micronuclei (d2-7 arrows), and anaphase bridges (d7-9 stars). (e) Bar graphs showing the percentage of nuclei with overt DDR, micronuclei, and anaphase bridges from a total number of 195-250 nuclei quantified for each genotype.

Figure 4. Telomeric DDR occurs at chromosome ends with detectable telomeric signal. (a) Metaphase TIF (indicated by white arrows) were analyzed by FISH-IF using a γH2AX (green) antibody and a telomeric C-probe (red). A total of 43 metaphases were countified for each M/M (PD 261) and I/I (PD 259) MEFs culture. Shown are the number of DDR foci per metaphase at signal-free (left) and telomeric (right) chromosome ends. The mean and SD for TIF are indicated by black lines. P values were calculated by two-tailed paired t-test. (b) Examples of abundant pairs of I/I MEFs nuclei that are connected by anaphase bridges and at least one nucleus of the pair displays overt DDR. The DAPI signal is enhanced to visualize the bridge. A total of 274 nuclei were counted for each M/M (PD 261) and I/I (PD 259) MEFs culture. The graph on the right shows the percentage of bridges between pairs with at least one damaged nucleus counted per field. The P value (0.001) was calculated by unpaired t-test, showing the mean and SD in black lines.

Figure 5. Increased telomeric and genomic aberrations in HHS MEFs. (a) Representative images for metaphase chromosomes of M/M and I/I MEFs at PD 250 respectively, hybridized with a red telomeric probe. Colored arrows indicate chromosomal aberrations as in (c). (b) Scatter plots showing the average number of each aberration type per metaphase (normalized to the number of chromosomes counted) at PD 250. Horizontal lines show mean and standard deviation. 619 chromosomes (15 metaphases) M/M PD250 and 692 chromosomes (17 metaphases) I/I PD 250 were quantified. P-values were calculated by unpaired two- tailed t-test. (c) Representative images of aberration types in I/I MEFs are shown: telomere loss (TL), telomere fragility, and interstitial telomere insertions (ITS). (d, e, f) Genomic

abnormalities associated with the M492I mutation, including connected nuclei, chromosome fragments, mitotic catastrophe, micronuclei and anaphase bridges.

Figure 6. Elevated homologous recombination between sister telomeres in HHS MEFs. (a) Chromatid-Orientation (CO)-FISH was performed on M/M and I/I MEFs at PD106 and PD104, respectively, labeling the leading and lagging telomeres with green and red using strand-specific PNA probes. 20 metaphases were quantified for each culture. Enlarged show examples of Telomere Sister Chromatid Exchange (T-SCE) events. (b) T-SCE events (indicated by arrows) were counted and presented as the percentage from the number of detectable telomeres in each metaphase. Horizontal lines show mean and standard deviation. P-value was calculated by two-tailed paired t-test.

Figure 7. HHS mouse telomeres progressively shorten over generations. Genomic DNA samples extracted from blood leukocytes (a) or tail (b) from HHS or WT mice at the indicated generations and ages were analyzed by PFGE and in-gel hybridization to the denatured DNA. Representative gels are indicated. Additional gels are shown in Figure S5. (c,d) MTL for each generation was repeatedly measured from blood (n= 35 for WT, n= 28 for HHS mice, and n= 83 for Telomouse) and tail (n= 38 for WT, n= 67 for HHS mice, and n= 150 for Telomouse) samples in independent gels and the results were plotted with the best-fit regression lines [4th order polynomial for tail and 2nd order polynomial for blood] (All data are summarized in Extended Data Table 2). Telomice MTL values[9] were added for comparison. The average age for HHS mice analyzed was 329 days, for Telomice, 331 days, and for WT mice, 355.5 days.

Figure 8. Structural models of the human and mouse RTEL1 helicase domains. (a) A model of the mouse helicase domain of RTEL1 generated by *AlphaFold*[35]. (b) Overlay of the human (wheat color) and mouse (pale green) RTEL1 helicase domains. V485 and L485, located in the same helix that contains M492 in the human and mouse RTEL1, respectively, are shown in 'stick' format. The displacement of this helix and the adjacent strand are highlighted in dashed boxes. (c) Interactions of the mouse M492 with the surrounding residues, and of K257 and E261 with the single-stranded DNA (ssDNA). (d) Interactions of the human M492 with the surrounding residues, and of K257 and E261 with the single-

stranded DNA (ssDNA). (e) Panel c is rotated 90˚ to show the positions of M492, L710 and G739, all of which are involved in POLDIP3 binding[37]. (f) Same as in e but for panel d.

METHODS

Derivation of *Rtel1*^{M492I} mice

CRISPR guide RNAs were designed as described[39]. For sgRNA preparation, the T7 promoter sequence was added to the sgRNA template by PCR amplification using pX335 (Addgene #42335) with Phusion high-fidelity DNA Polymerase Kit (NEB), Common sgRNA-R and Primer 1 or Primer 2 (see below).

Common sgRNA-R: 5'-AGCACCGACTCGGTGCCACT-3'

Primer 1 with gRNA sequence underlined:

5'-TTAATACGACTCACTATAGGCATCTGCATCTCCAGAGCAAgttttagagctagaaatagc-3'

Primer 2 with gRNA sequence underlined:

5'-TTAATACGACTCACTATAGGCACCTGGAGGTCACAACACTgttttagagctagaaatagc-3'

PCR products were purified using the QIAquick Gel Extraction kit (Qiagen), followed by in vitro transcription with the T7 High Yield RNA Synthesis kit (NEB). Newly synthesized sgRNAs were purified using the MEGAclear kit (Life Technologies), precipitated and diluted in injection buffer (10 mM Tris / 0.1 mM EDTA, pH 7.5) at a concentration of 500 ng/µl. The quality of the sgRNAs was confirmed using the total RNA Nano Chip on an Agilent bioanalyzer. The final injection mix was prepared using ssDNA repair template (IDT; 100 ng/µl), sgRNA1 (50 ng/µl), sgRNA2 (50 ng/µl), and Cas9 Nickase mRNA (Trilink; 100 ng/µl) in injection buffer. The sequence of the ssDNA repair template is shown below.

5'-GTTCGTACCCTTATCCTCACCAGCGGTACCCTGGCTCCACTGTCTTCCTTTGCTCTGGAGAAGCAGATGTATG TATGAGTCACCTGGAGGTCACAACACTAGGAACATGGTGGGTGGGGTTGG-3'

The final mix was spun twice at top speed for 30 minutes at 4˚C to remove debris to avoid needle clogging. Cytoplasmic injection was done using C57Bl6 zygotes. After injection, SCR7 (Xcessbio) was added to the overnight egg culture at the concentration of 50 µM. Out of the 15 mice born, one had the targeted allele.

Preparation and culture of MEF

Embryonic day (E)13.5 mouse embryos were dissected with head and inner organs removed, rinsed in HBSS, then digested with 300 µl papain isolation enzyme (ThermoFisher) for 30 minutes at 37˚C following the manufacturer's protocol. Embryonic digests were transferred to conical tubes with 1 ml of HBSS, pipetted up and down to achieve single cell suspension and then spun. The pellets were resuspended in MEFs media (DMEM with 20% FCS, Pen/Strep/non-essential amino acids) and plated. MEFs were grown in DMEM media containing 2 mM L-glutamine, penicillin-streptomycin, non-essential amino acids and 20% fetal bovine serum until immortalization (around PD60-70) and then with 10% fetal bovine serum in the same medium. BIOAMF-2 complete media was used for poorly growing I/I cultures at early PD, then 20% fetal bovine serum was used. All media and media supplements were purchased from Biological Industries Inc., Beit Haemek, Israel.

Culture of S2 human fibroblasts

Fibroblasts derived from HHS-patients were grown in DMEM media supplemented with 10% fetal bovine serum, penicillin-streptomycin, 2mM L-glutamine and non-essential amino acids. To induce the ectopic expression of hRTEL1, the medium was supplemented with 30 ng/ml doxycycline (Dox). To silence its expression, Dox was omitted from the medium and a certified tetracycline-free fetal bovine serum was used. Media and media supplements were purchased from Biological Industries Inc. Beit Haemek, Israel.

Genomic DNA extraction

Leukocytes were obtained from mouse blood by lysing red blood cells in 155 mM NH4Cl, 10 mM KHCO3 and 0.1 mM EDTA pH 8 followed by centrifugation. Mouse leukocytes, MEFs, and S2 human fibroblasts were lysed in 10 mM Tris pH 7.5, 10 mM EDTA, 0.15 M NaCl, 0.5% SDS and 100 µg/ml proteinase K overnight at 37˚C. Mouse tail samples were lysed in 100 mM Tris HCl pH 8.5, 5 mM EDTA, 0.1% SDS, 200 mM NaCl and 100 µg/ml proteinase K overnight at 50˚C. Following cell lysis, high molecular weight genomic DNA was phenol-extracted, ethanol-precipitated, and dissolved in TE. Genomic DNA samples were examined by agarose gel electrophoresis of undigested DNA, and samples suspected to be degraded were excluded from further analysis.

In-gel analysis of telomeric restriction fragments

Genomic DNA was treated with RNase A, digested with the HinfI restriction endonuclease, and quantified by Qubit fluorometer. Equal amounts (1-5 µg) of the digested DNA samples were separated by pulsed-field gel electrophoresis (PFGE) using a Bio-Rad CHEF DR-II apparatus in 1% agarose and 0.5 x TBE, at 14˚C, 200V and pulse frequency gradient of 1 sec (initial) to 6 sec (final) for 18-22 hr, or in regular gel apparatus, 0.7% agarose and 1 x TBE for 1,300 V x hr. Gels were ethidium-stained, dried and hybridized as previously described[9]. Probe mixtures contained a telomeric oligonucleotide (AACCCT)3, and mid-range PFG ladder (for mouse samples) (NEB Inc.) and 1 kb ladder (GeneDirex Inc.), which were digested with HinfI, dephosphorylated by quick calf intestinal phosphatase (NEB Inc.) and heat inactivated. All probes were 5' end-labeled with [alpha-32P]-ATP and T4 polynucleotide kinase (NEB Inc.). The gels were exposed to a Phosphor Imager. TRF length was quantified using TeloTool (corrected mode) as previously described[9]. Native and denatured in-gel hybridization intensities were quantified using ImageQuant-TL (GE Healthcare Inc.).

2D gel hybridization

Genomic DNA was treated with RNase A, digested with the HinfI restriction endonuclease, and quantified by Qubit fluorometer. In the first dimension, Equal amounts (~ 20-25 µg) of the digested DNA samples were separated by PFGE using a Bio-Rad CHEF DR-II apparatus as described previously, but in 0.4% agarose and 0.5 x TBE, at 20˚C, 35V and pulse frequency gradient of 1 sec (initial) to 6 sec (final) for 50 hr. The gel was stained with ethidium bromide and visualized by UV light. The appropriate lanes were then excised for the second-dimension run. A 1.1% pulsed-field agarose gel in 0.5 XTBE containing 3% ethidium bromide was poured around the excised slab, and the second-dimension electrophoresis was carried out in the same apparatus at at 14˚C, 200V and pulse frequency gradient of 1 sec (initial) to 6 sec (final) for 20-22 hr. The gel was then visualized using UV light, dried, hybridized as previously described in the In-gel analysis of telomeric restriction fragments, and exposed to a Phosphor Imager.

Restriction fragment length PCR (RFLP) to verify MEFs genotypes

PCR reaction was performed on the MEFs (50-100 ng gDNA) giving a product of 269 bp, using the following primers in 25µl reaction (annealing Tm 58; extension 72' 15''; 35 cycles):

1- mRtel1gM492UP 5'-CAGTCCCAGCCAGAGTATGC-3'

2- mRtel1gM492LP 5'-AATGGACTGGGAATGGCCAG-3'

The products were cut by *HinfI* restriction enzyme, giving the following results according to the genotypes: M/M: 117+152 bp, M/I:100+117+152 bp, I/I: 100+17+152 bp

Western Blot

Western blot was done as previously described[8], but using alpha tubulin antibodies as loading control.

Immunofluorescence of cultured cells

Cells were seeded onto glass coverslips and grown for 1-4 days. Immunofluorescence was done as described[8]. Imaging was performed using FV-1200 confocal microscope (Olympus, Japan) with a 60X/1.42 oil immersion objective. NIH ImageJ28 was used for image analysis and foci quantification.

Meta-TIF assay

Meta-TIF was performed as previously described[9], and Images were acquired using the Olympus IX83 fluorescence microscope system (Olympus).

Metaphase FISH

Metaphase spreads and FISH were performed as previously described[9], using TelC-Alexa488 telomeric probe (F1004, Panagene Inc) or TelC-Cy3 probe (F1002-5, Panagene). Imaging acquisition was done by Olympus IX83 fluorescence microscope system (Olympus).

Chromosome-Orientation Fluorescent In-Situ Hybridization (CO-FISH)

The protocol was done as previously described[9], and Images were acquired using the Olympus IX83 fluorescence microscope system (Olympus).

Generating a three-dimensional structure model of the murine and human RTEL1 helicase domain

There are no available structures of the full length RTEL1 from any organism. The only structures of RTEL1 currently available publicly are those of the Harmonin-homology domain 2 (HHD2) of human RTEL1 (RCSB PDB ID: 7WU8) and the full-length model generated by the artificial intelligence software

AlphaFold[35] (human AF-Q9NZ71-F1 and Mouse AF-Q0VGM9-F1). Structural comparison of the Alphafold generated RTEL1 helicase domain with that generated by the *Protein Homology Recognition Engine Phyre 2*[9,40] shows striking similarity between the 2 structures so we used the *AlphaFold* structure of the helicase domain of human and mouse RTEL1 for our analysis. Similarly to our previous RTEL1 M492K study, the positioning of the single stranded DNA at the RTEL1 helicase domain was predicted using an overlay of the *AlphaFold* RTEL1 model with its closest structural homolog, the crystal structure of the DinG XPD family helicase in complex with single stranded DNA (ssDNA; RCSB PDB ID: 6FWS[10]). The *AlphaFold* Helicase domain of human and mouse RTEL1 bound to ssDNA was used for any subsequent analysis.

Mice

DNA samples from a total of 48 I/I and 24 M/M (100% pure C57BL/6) mice were analyzed multiple times in separate gels (as detailed in Extended Data Table 2). The average age for I/I mice analyzed in the gels was 329.0 days, while the average age for M/M mice was 355.5 days. At each specific generation of breeding, the following mice were analyzed:

F0 (M/M): 24 mice (63 - 665) days old,

F2 (I/I): two mice 355 and 433 days old,

F3 (I/I): 6 mice (115 – 1014) days old,

F4 (I/I): 7 mice (174 – 738) days old,

F5 (I/I): 5 mice (149 – 505) days old,

F6 (I/I): 4 mice (48 – 455) days old,

F7(I/I): 6 mice 38 days old,

F8 (I/I): 5 mice 215 days old,

F9 (I/I): 2 mice 239 days old,

F10 (I/I):10 mice (53 – 154) days old,

F11 (I/I): one mouse 80 days old.

Four mouse embryonic fibroblast cultures were grown over 250 population doublings (PD) and sampled at different PD. Samples were analyzed in gels, as detailed in Extended Data Table 1.

Data availability

All measured and calculated values are provided in the Extended Data Tables 1 (MEFs) and 2 (mice). Additional gel replicates and data are available upon request to the corresponding authors.

Statistical analysis

Statistical analysis was performed by Microsoft Excel and GraphPad Prism 8.0, using simple linear, polynomial, or segmental linear regression with setting the break points manually to give the best fit by coefficient of determination (R2). For statistical tests two-tailed paired or unpaired t-test were used, as indicated for each figure. $P < 0.05$ was considered statistically significant.

SUPPLEMENTARY FIGURE LEGENDS

Figure S1. Conservation of the RTEL1 helicase domain between human and mouse. Protein sequence alignment of the RTEL1 helicase domain, including HD1, HD2, the iron-sulfur (FeS) and the ARCH domains, showing high conservation between human and different mouse species (*M. musculus, M. castaneus, M. spretus, M. caroli*, and *M. pahari*). The red arrow shows Codon 492, which encodes the conserved methionine, with a lysine variation in *M. spretus*, mutated to isoleucine in HHS.

Figure S2. Silencing the ectopic expression of WT hRTEL1v2 progressively shortened the telomeres of human patient fibroblasts carrying the *RTEL1*^{M492I} mutation. (a) S2-hTERT-TPP1 fibroblast culture[8] was grown for 58 PD in the presence of 30 ng/ml doxycycline (DOX) to induce the expression of FLAG-tagged RTEL1v2, and then without Dox for 10 PDs. Then the culture was split; half continued to grow in the absence of DOX while the other half was grown with DOX. From this point, PD level was plotted over time in culture till reaching PD 100 with or without DOX. (b) genomic DNA prepared from the S2-hTERT-TPP1-RTEL1v2 cultures (+/-DOX) at the indicated PD were analyzed by in-gel hybridization. Shown is the hybridization of the telomeric probe to the denatured DNA. MTL values, measured by *Telotool*[38], are indicated below the lanes for each sample. (c) Cell morphology and western analysis using anti-FLAG antibody to detect the FLAG-tagged RTEL1v2 in these S2-hTERT-TPP1 fibroblasts. Alpha -tubulin was used as a loading control.

Figure S3. Genotyping of M/M, M/I, and I/I MEFs. The genotypes of the MEFs cultures were confirmed at PD 250 by restriction fragment length PCR (RFLP). PCR products were digested with *HinfI* restriction endonuclease. An additional restriction site formed by the M492I mutation shortens the 117 bp fragment by 17 bp.

Figure S4. Immortalization and growth characteristics of MEFs from WT and Rtel1M492I mutant mice. (a) MEFs cultures were prepared from F3 littermate embryos, I/I, M/I and M/M*, generated by mating F2 heterozygous mice carrying the *Rtel1*^{M492I} mutation. Another control M/M MEFs culture (M/M) was generated by intercrossing WT mice which did not have any *Rtel1* mutation in their pedigree, to avoid trans-generational inheritance of short telomeres from the heterozygous mice to the WT offspring. All four cell lines were immortalized by serial passaging and grown to PD 250. Arrows indicate different growth phases which are shown as bars in (b). (b) Growth rates were calculated based on the graphs in (a) and indicated above the bars. Days, PD, and coefficient of determination (R2), for the linear regression line calculated for each growth phase are indicated below. **** indicating $P < 0.0001$ and *** indicating $P<0.001$. (c) Representative images show different cell morphology for the different cultures before and after immortalization.

Figure S5. The HHS mouse telomeres progressively shorten over generations. Genomic DNA samples extracted from tail (a) or blood leukocytes (b) from mutant (I/I) or WT (M/M) mice at the indicated generations and ages were analyzed by PFGE and in-gel hybridization to the denatured DNA. Gel examples are shown.

Figure S6. No increase in t- circle levels in Telomouse and HHS mouse. (a,b) gDNA (~20-25 µg) extracted from HHS mouse (I/I) and Telomouse (K/K) tail at the same generation (F5), as well as from WT mouse (M/M) was digested with *HinfI* and separated by two-dimensional (2D) PFGE as detailed in the "Methods" section. Shown are two gels, each containing two tail DNA samples: M/M & K/K in (a), and I/I & K/K (same as in (a)) in (b). The same Ethidium staining shows all genomic DNA fragments. Telomeric circles were detected by in-gel hybridization with a C-rich radioactive probe and visualized using a Phosphor-Imager. Short exposure shows comparable amounts of telomeric DNA in each sample.

The green and red arrows indicate linear- and circular-form of telomeric DNA, respectively. (c) A scheme showing the 2D gel principle.

EXTENDED DATA LEGENDS

Extended Data Table 1. Mouse embryonic fibroblasts. Genomic DNA samples, prepared from WT (M/M, M/M*), homozygous mutant (I/I) or heterozygous (M/I) for the *Rtel1*^{M492I} mutation, were grown over 250 population doublings (PD), sampled at different PD, and analyzed in ten different gels by PFGE and in-gel hybridization to the denatured DNA. Mean telomere length was quantified using *TeloTool*[38] using the 'corrected' mode. Percentage of telomeres below 15 kb (TL< 15) or 20 kb (TL<20) was calculated from the mean TRF length and the standard deviation (SD).

Extended Data Table 2. Mice. Genomic DNA samples from 48 I/I and 24 M/M (100% pure Blk6 C57BL/6) mice were analyzed multiple times in separate gels PFGE (as indicated) and in-gel hybridization to the denatured DNA. Mean telomere length was quantified using *TeloTool*[38] using the 'corrected' mode. Percentage of telomeres below 15 kb (TL< 15) or 20 kb (TL<20) was calculated from the mean TRF length and the standard deviation (SD). The average age for I/I mice analyzed was 329.0 days, while the average age for M/M mice was 355.5 days. At each specific generation, the following mice were analyzed:

F0 (M/M): 24 mice (63 - 665) days old

F2 (I/I): two mice 355 and 433 days old

F3 (I/I): 6 mice (115 – 1014) days old

F4 (I/I): 7 mice (174 – 738) days old

F5 (I/I): 5 mice (149 – 505) days old

F6 (I/I): 4 mice (48 – 455) days old

F7(I/I): 6 mice 38 days old

F8 (I/I): 5 mice 215 days old

F9 (I/I): 2 mice 239 days old

F10 (I/I):10 mice (53 – 154) days old

F11 (I/I): one mouse 80 days old

FIGURES

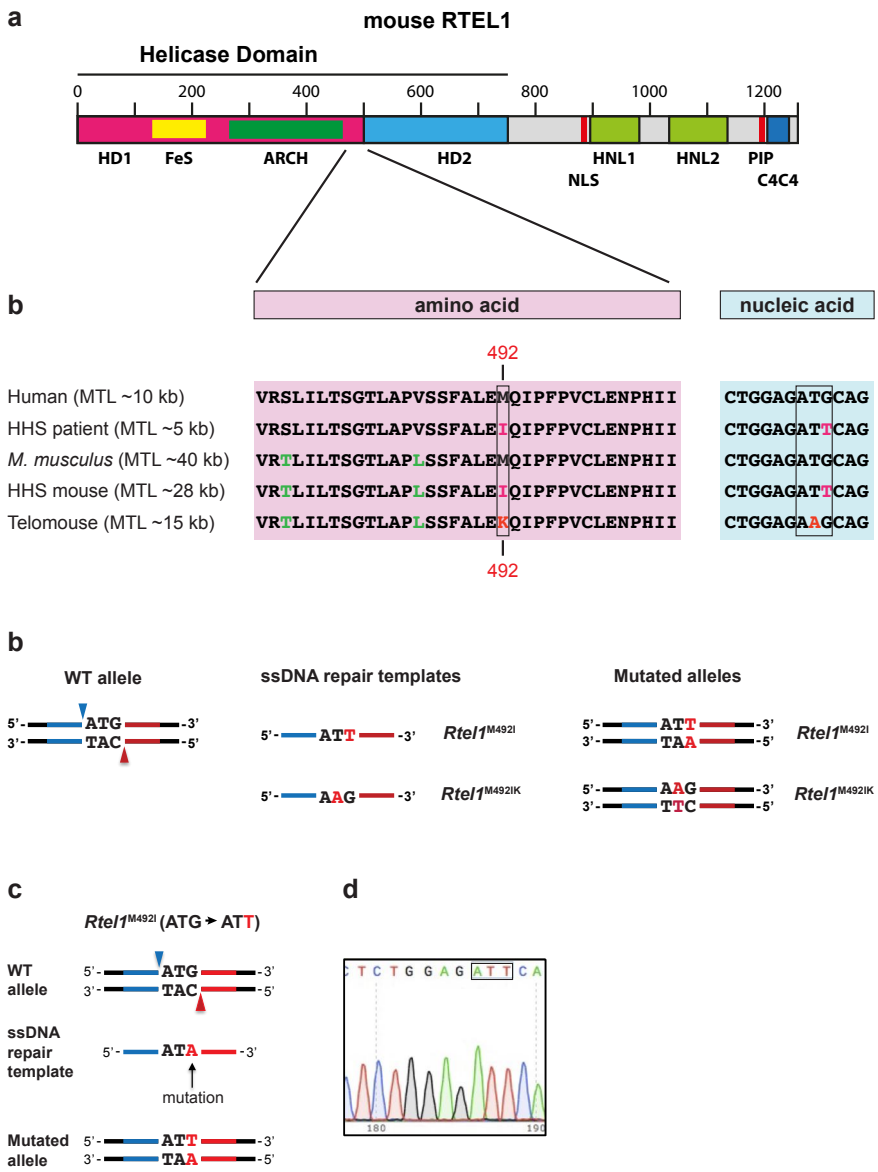

Figure 1. Derivation of the Rtel1^{M492I} allele by CRISPR-Cas9 nickase editing. (a) A scheme showing the helicase domains (HD1 and HD2), the iron-sulfur cluster (FeS), the nuclear localization signal (NLS), harmonin N-like domains (HNL1 and HNL2), PCNA-interacting protein (PIP) motif, and the C4C4 ring-finger domain[12] of RTEL1. (b) RTEL1 protein and DNA sequence alignment showing codon 492 (boxed) and flanking sequences in human and mouse. Variations in mouse from the human sequence are shown in green and mutations in HHS patients and mouse models are shown in red. The mean telomeric restriction fragment (TRF) length (MTL) values measured by the in-gel hybridization method are indicated for human and mouse. (c) Illustration showing the WT allele, the two positions targeted by gRNAs (blue and red arrowheads), the ssDNA repair template with the mutation, left homology arm (blue), right homology arm (red), and the resulting targeted allele. (d) Sanger sequencing of the HHS line founder confirming the replacement of the 'G' with a 'T' in codon 492, changing the methionine to an isoleucine (underlined).

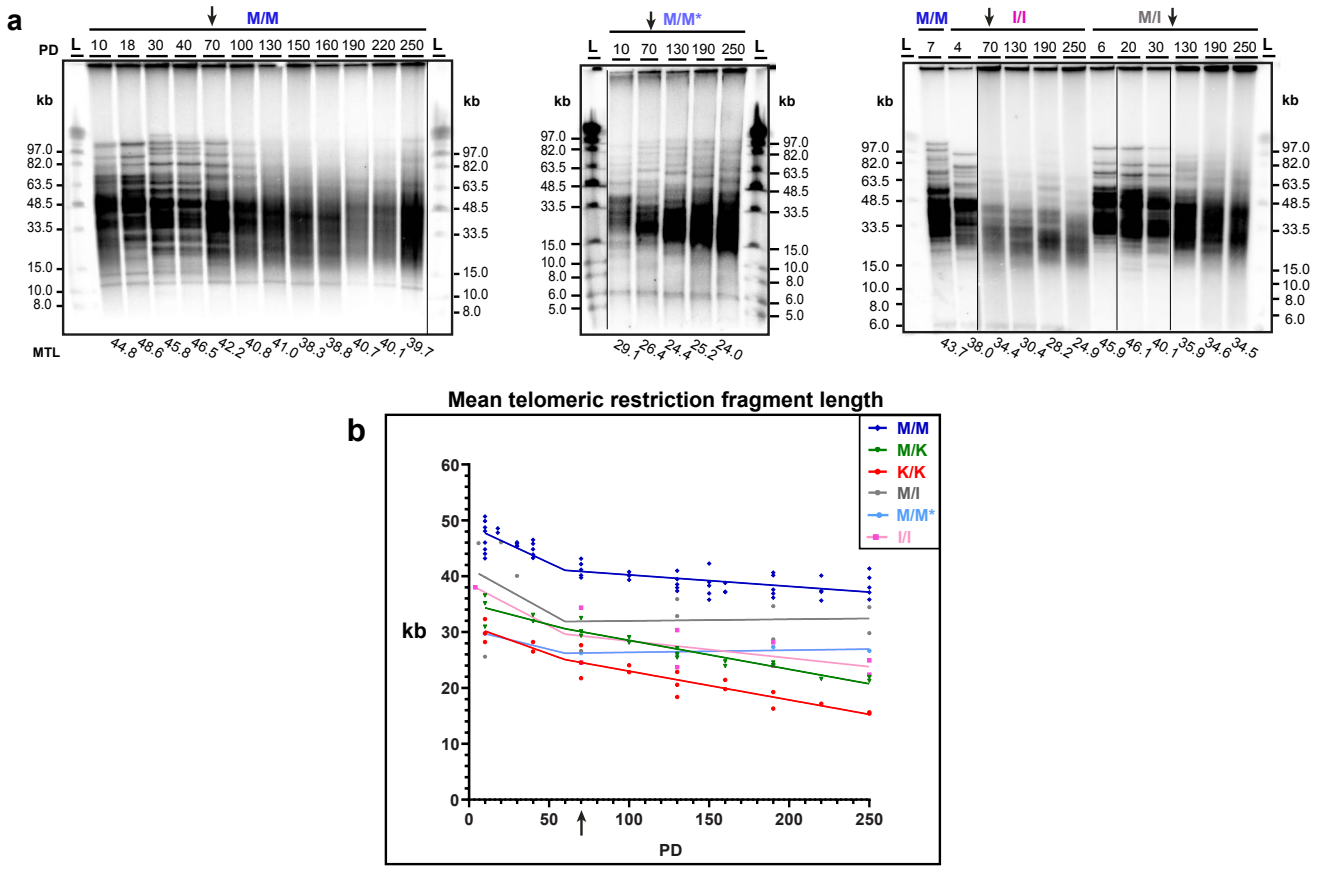

Figure 2. Telomeres of MEFs carrying the homozygous *Rtel1*^{M492I} mutation progressively shorten with cell division in culture. MEFs cultures were prepared from F3 littermate embryos, I/I, M/I and M/M*, generated by mating F2 heterozygous mice carrying the Rtel1 M492I mutation. Another control M/M MEFs culture (M/M) was generated by intercrossing WT mice which did not have any Rtel1 mutation in their pedigree, to avoid trans-generational inheritance of short telomeres from heterozygous *Rtel1* mutant mice to the WT offspring. All four cell lines were immortalized by serial passaging and grown to PD 250. (a) Genomic DNA samples extracted from the indicated MEFs cultures and PDs were digested by *HinfI* restriction endonuclease and analyzed by PFGE and in-gel hybridization with a C-rich telomeric probe. Shown is the hybridization after denaturation (see Methods). Mean TRF length (MTL) was quantified for each sample by *TeloTool*[38] and indicated below the lanes. (b) All MTL values measured in multiple gels for the same M/M, I/I, and M/I MEFs samples were plotted, in addition to K/K and M/K MEFs results from[9], for comparison.

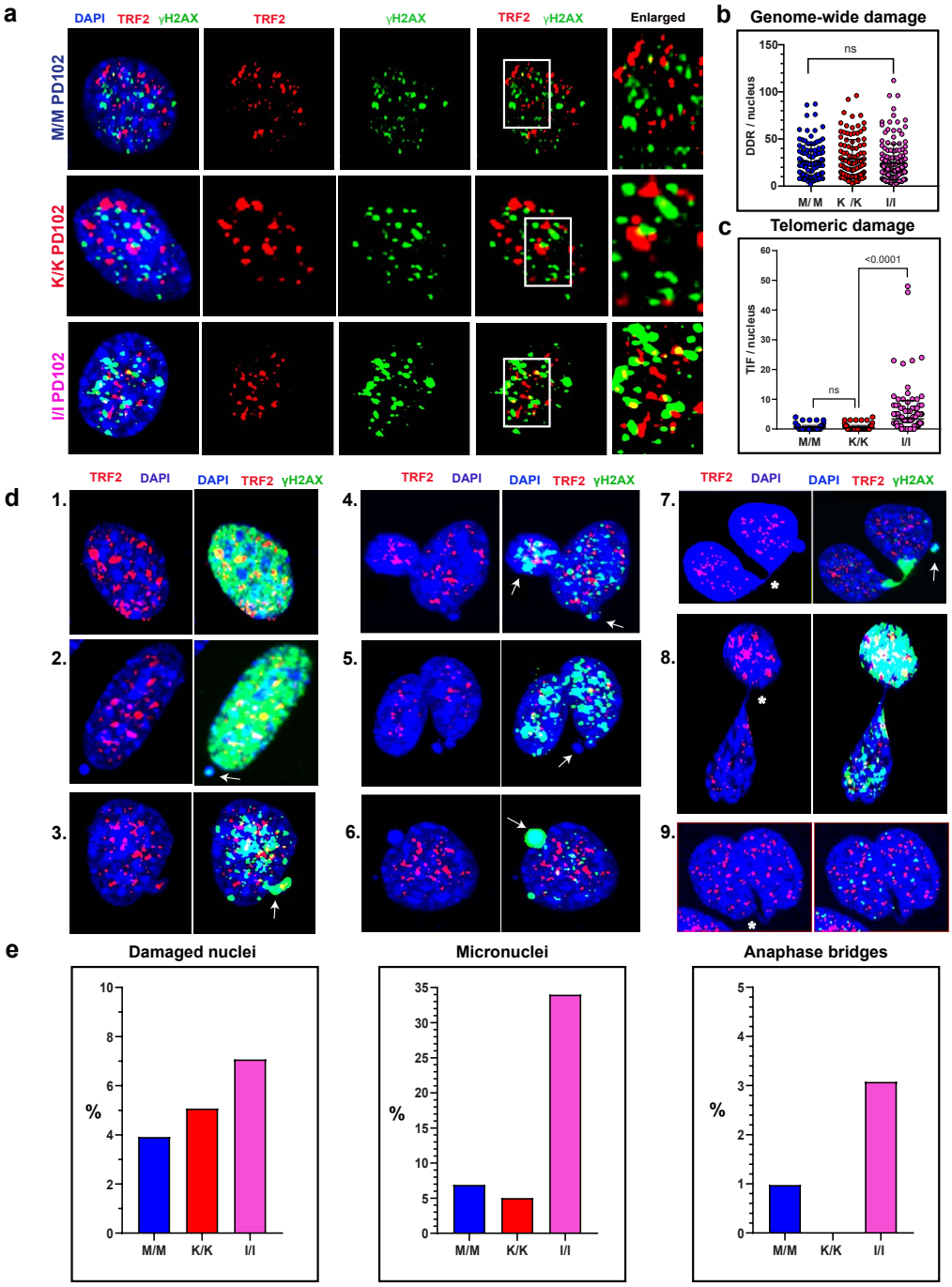

Figure 3. The HHS mutation impairs telomere protection and genome stability. (a) The formation of DNA damage response foci and their localization to telomeres (defined as TIF) in interphase nuclei were examined by immunofluorescence staining with antibodies detecting the DDR marker γH2AX (green) and the telomere protein TRF2 (red). Scatter plots show the number of DDR foci (b) and TIF (c) per nucleus. A total of 110 M/M, 110 K/K, and 153 (b) or 182 (c) of I/I nuclei were countified for MEFs PD 102. All three MEFs cultures were analyzed side by side; the results for the K/K and control (M/M) MEFs appeared in[9]. The mean values and SDs are indicated by black lines, and P values were calculated by unpaired t-test. (d) Representative images showing nuclei with overt DDR (d1,2), micronuclei (d2-7 arrows), and anaphase bridges (d7-9 stars). (e) Bar graphs showing the percentage of nuclei with overt DDR, micronuclei, and anaphase bridges from a total number of 195-250 nuclei quantified for each genotype.

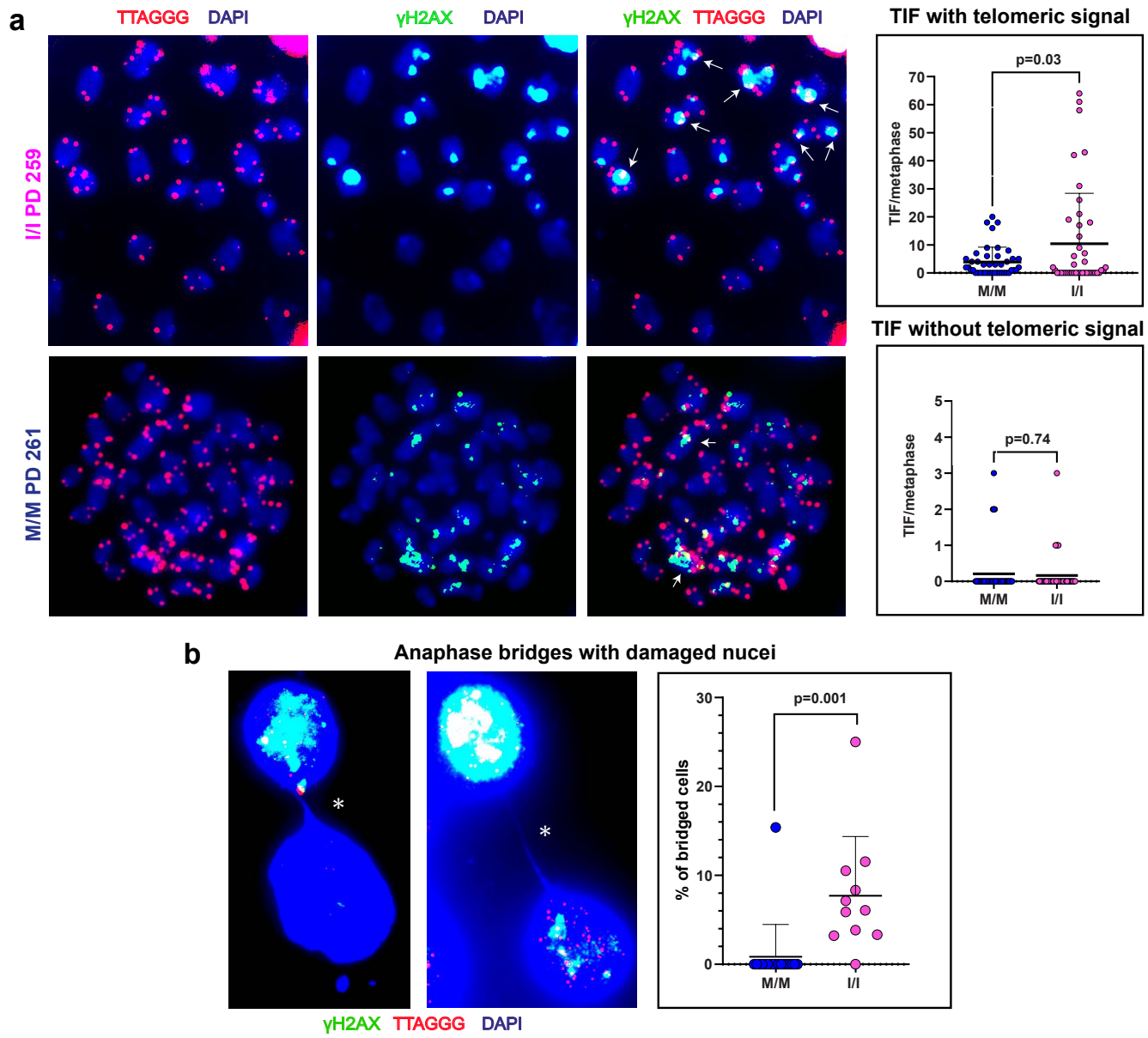

Figure 4. Telomeric DDR occurs at chromosome ends with detectable telomeric signal. (a) Metaphase TIF (indicated by white arrows) were analyzed by FISH-IF using a γH2AX (green) antibody and a telomeric C-probe (red). A total of 43 metaphases were countified for each M/M (PD 261) and I/I (PD 259) MEFs culture. Shown are the number of DDR foci per metaphase at signal-free (left) and telomeric (right) chromosome ends. The mean and SD for TIF are indicated by black lines. P values were calculated by two-tailed paired t-test. (b) Examples of abundant pairs of I/I MEFs nuclei that are connected by anaphase bridges and at least one nucleus of the pair displays overt DDR. The DAPI signal is enhanced to visualize the bridge. A total of 274 nuclei were counted for each M/M (PD 261) and I/I (PD 259) MEFs culture. The graph on the right shows the percentage of bridges between pairs with at least one damaged nucleus counted per field. The P value (0.001) was calculated by unpaired t-test, showing the mean and SD in black lines.

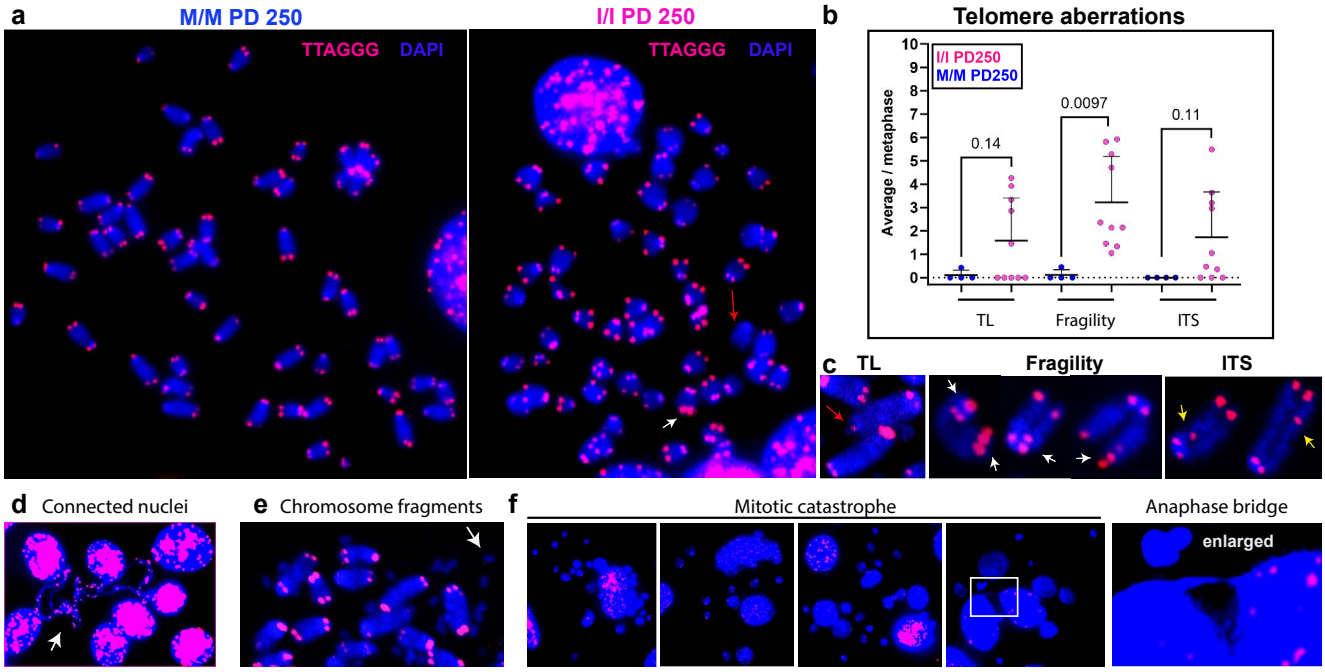

Figure 5. Increased telomeric and genomic aberrations in HHS MEFs. (a) Representative images for metaphase chromosomes of M/M and I/I MEFs at PD 250 respectively, hybridized with a red telomeric probe. Colored arrows indicate chromosomal aberrations as in (c). (b) Scatter plots showing the average number of each aberration type per metaphase (normalized to the number of chromosomes counted) at PD 250. Horizontal lines show mean and standard deviation. 619 chromosomes (15 metaphases) M/M PD250 and 692 chromosomes (17 metaphases) I/I PD 250 were quantified. P-values were calculated by unpaired two- tailed t-test. (c) Representative images of aberration types in I/I MEFs are shown: telomere loss (TL), telomere fragility, and interstitial telomere insertions (ITS). (d, e, f) Genomic abnormalities associated with the M492I mutation, including connected nuclei, chromosome fragments, mitotic catastrophe, micronuclei and anaphase bridges.

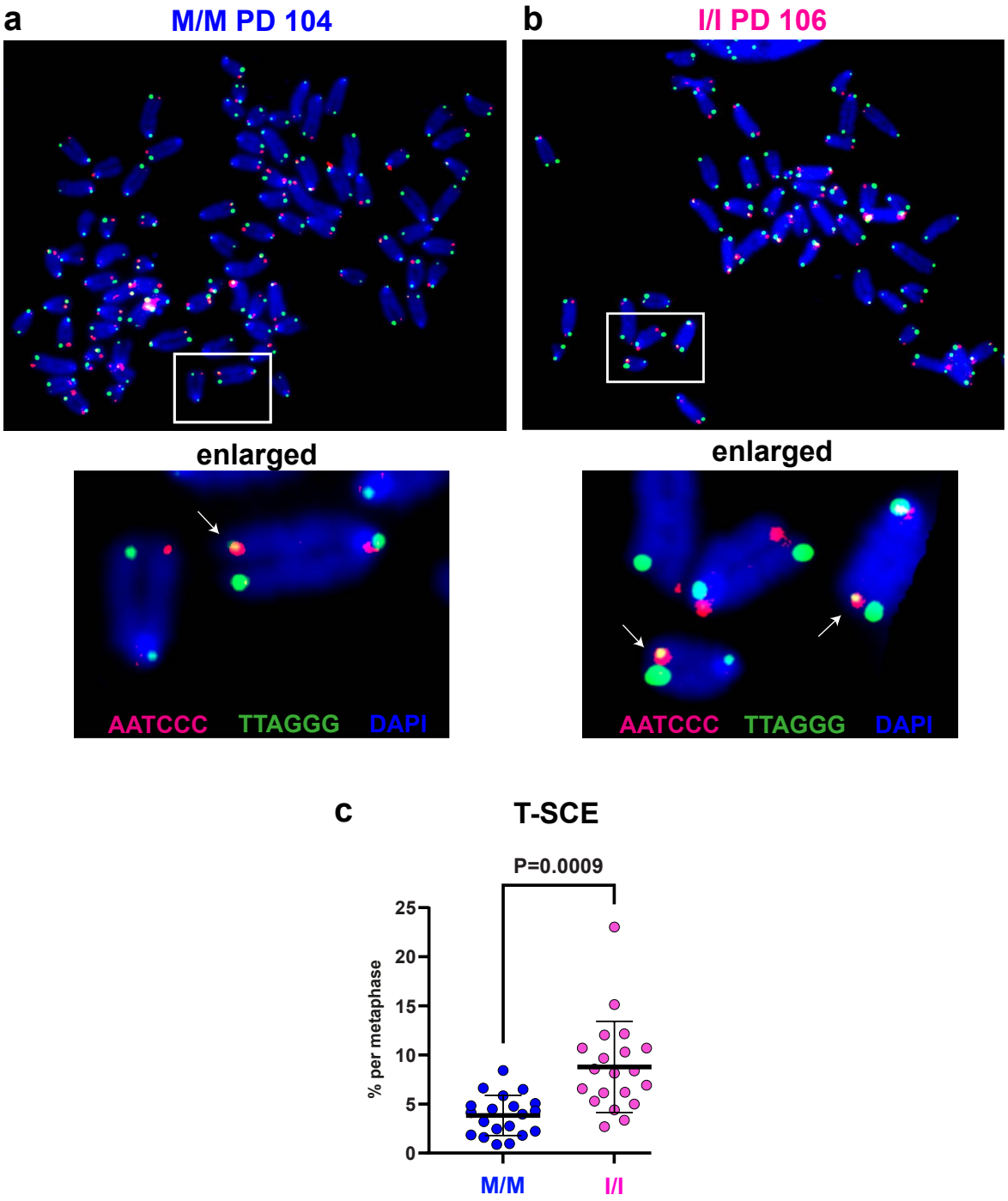

Figure 6. Elevated homologous recombination between sister telomeres in HHS MEFs. (a) Chromatid-Orientation (CO)-FISH was performed on M/M and I/I MEFs at PD106 and PD104, respectively, labeling the leading and lagging telomeres with green and red using strand-specific PNA probes. 20 metaphases were quantified for each culture. Enlarged show examples of Telomere Sister Chromatid Exchange (T-SCE) events. (b) T-SCE events (indicated by arrows) were counted and presented as the percentage from the number of detectable telomeres in each metaphase. Horizontal lines show mean and standard deviation. P-value was calculated by two-tailed paired t-test.

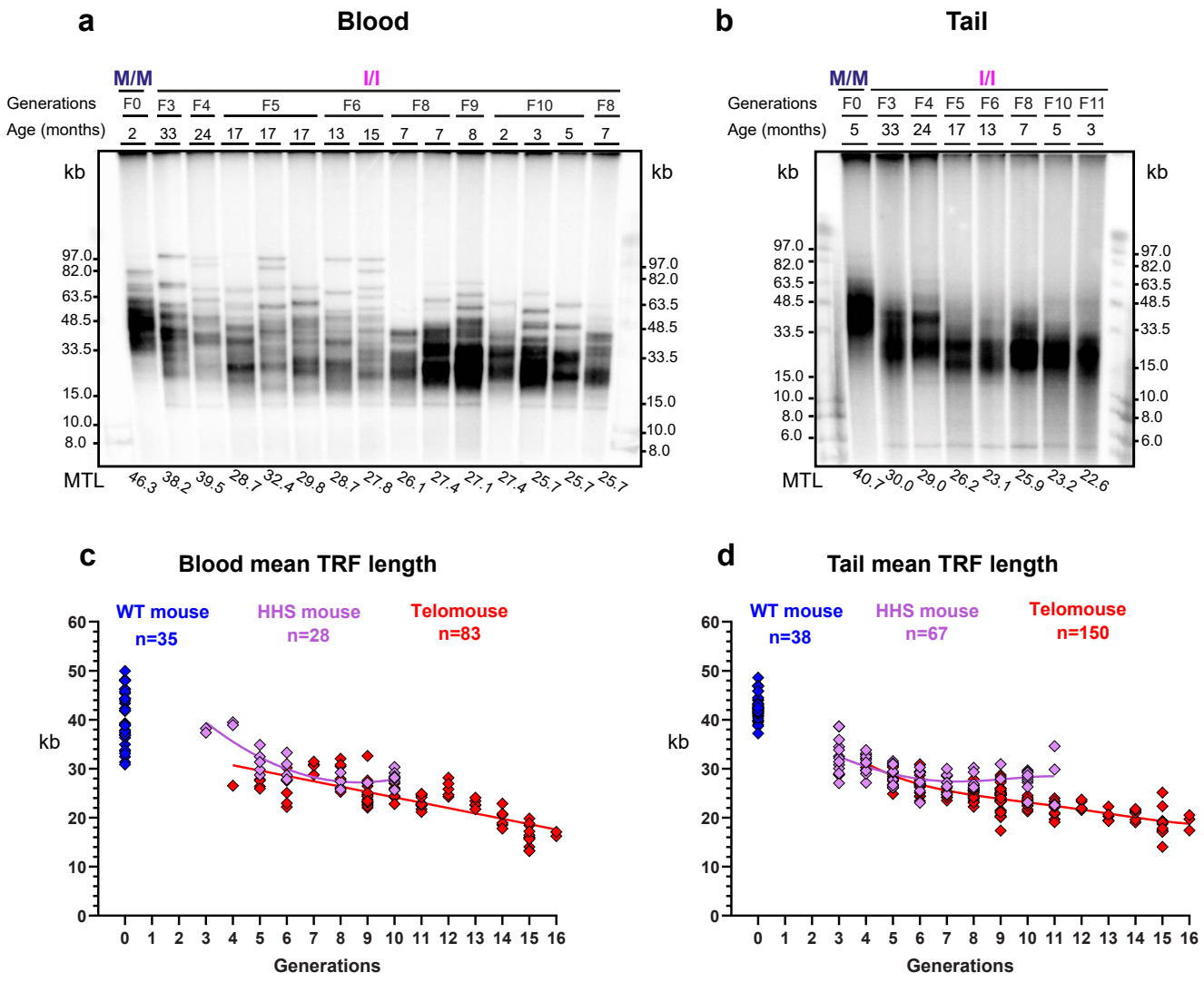

Figure 7. HHS mouse telomeres progressively shorten over generations. Genomic DNA samples extracted from blood leukocytes (a) or tail (b) from HHS or WT mice at the indicated generations and ages were analyzed by PFGE and in-gel hybridization to the denatured DNA. Representative gels are indicated. Additional gels are shown in Figure S5. (c,d) MTL for each generation was repeatedly measured from blood (n= 35 for WT, n= 28 for HHS mice, and n= 83 for Telomouse) and tail (n= 38 for WT, n= 67 for HHS mice, and n= 150 for Telomouse) samples in independent gels and the results were plotted with the best-fit regression lines [4th order polynomial for tail and 2nd order polynomial for blood] (All data are summarized in Table S2). Telomice MTL values[9] were added for comparison. The average age for HHS mice analyzed was 329 days, for Telomice, 331 days, and for WT mice, 355.5 days.

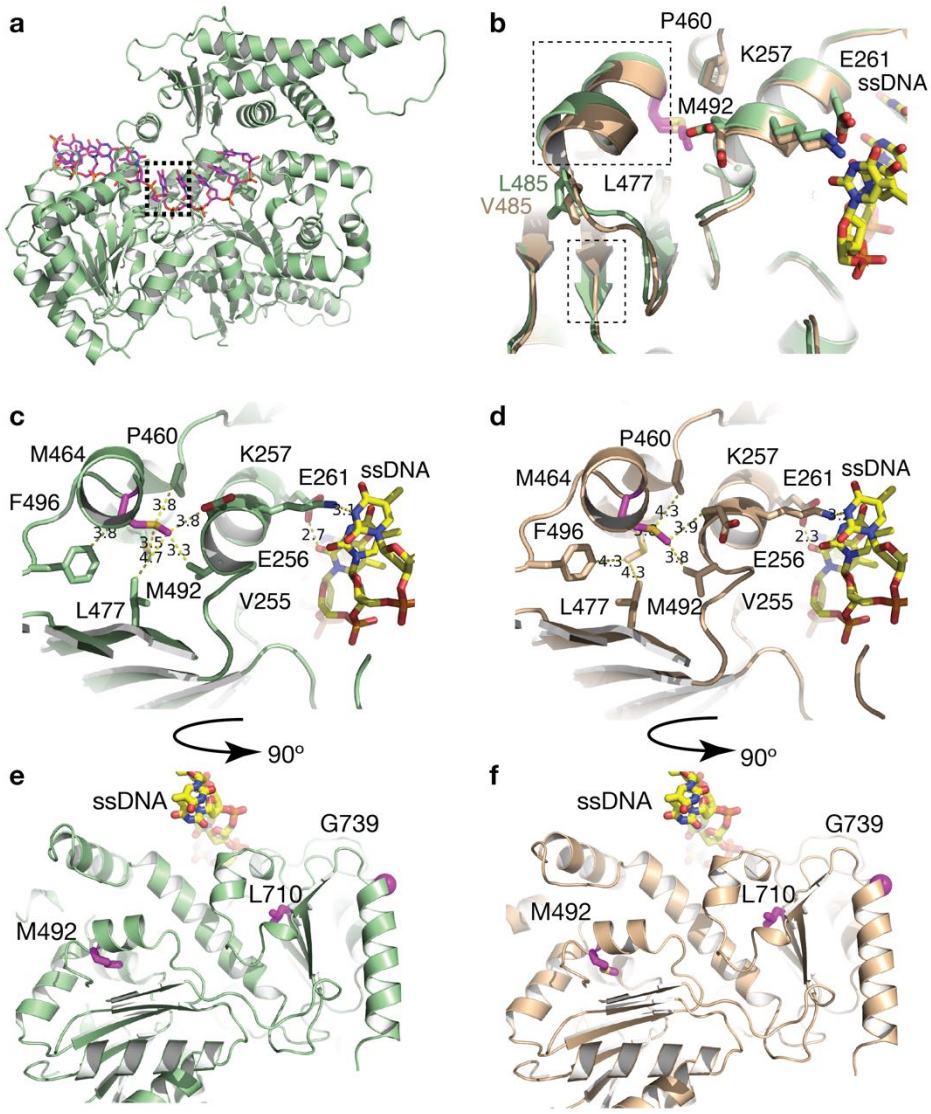

Figure 8. Structural models of the human and mouse RTEL1 helicase domains. (a) A model of the mouse helicase domain of RTEL1 generated by *AlphaFold*[35]. (b) Overlay of the human (wheat color) and mouse (pale green) RTEL1 helicase domains. V485 and L485, located in the same helix that contains M492 in the human and mouse RTEL1, respectively, are shown in 'stick' format. The displacement of this helix and the adjacent strand are highlighted in dashed boxes. (c) Interactions of the mouse M492 with the surrounding residues, and of K257 and E261 with the single-stranded DNA (ssDNA). (d) Interactions of the human M492 with the surrounding residues, and of K257 and E261 with the single-stranded DNA (ssDNA). (e) Panel c is rotated 90˚ to show the positions of M492, L710 and G739, all of which are involved in POLDIP3 binding[37]. (f) Same as in e but for panel d.